

## ORIGINAL ARTICLE

# Trade-offs between microbiome diversity and productivity in a stratified microbial mat

Hans C Bernstein<sup>1,2,3</sup>, Colin Brislawn<sup>2</sup>, Ryan S Renslow<sup>2,3</sup>, Karl Dana<sup>1</sup>, Beau Morton<sup>2</sup>, Stephen R Lindemann<sup>2</sup>, Hyun-Seob Song<sup>2</sup>, Erhan Atci<sup>3</sup>, Haluk Beyenal<sup>3</sup>, James K Fredrickson<sup>2</sup>, Janet K Jansson<sup>2</sup> and James J Moran<sup>1</sup>

<sup>1</sup>Chemical and Biological Signature Science, Pacific Northwest National Laboratory, Richland, WA, USA;

<sup>2</sup>Biological Sciences Division, Pacific Northwest National Laboratory, Richland, WA, USA and <sup>3</sup>The Gene and Linda Voiland School of Chemical Engineering and Bioengineering, Washington State University, Pullman, WA, USA

**Productivity is a major determinant of ecosystem diversity. Microbial ecosystems are the most diverse on the planet yet very few relationships between diversity and productivity have been reported as compared with macro-ecological studies. Here we evaluated the spatial relationships of productivity and microbiome diversity in a laboratory-cultivated photosynthetic mat. The goal was to determine how spatial diversification of microorganisms drives localized carbon and energy acquisition rates. We measured sub-millimeter depth profiles of net primary productivity and gross oxygenic photosynthesis in the context of the localized microenvironment and community structure, and observed negative correlations between species richness and productivity within the energy-replete, photic zone. Variations between localized community structures were associated with distinct taxa as well as environmental profiles describing a continuum of biological niches. Spatial regions in the photic zone corresponding to high primary productivity and photosynthesis rates had relatively low-species richness and high evenness. Hence, this system exhibited negative species–productivity and species–energy relationships. These negative relationships may be indicative of stratified, light-driven microbial ecosystems that are able to be the most productive with a relatively smaller, even distributions of species that specialize within photic zones.**

*The ISME Journal* (2017) 11, 405–414; doi:10.1038/ismej.2016.133; published online 1 November 2016

## Introduction

The majority of primary producers on the planet are powered by oxygenic photosynthesis and their rates of carbon fixation typically set the upper bound for ecosystem productivity (Field *et al.*, 1998). Communities exhibiting the highest net rates of primary productivity should produce the most biomass. However, the question remains as to whether higher-species diversity results in greater rates of biological energy and carbon acquisition. Ecological theories, such as the maximum power principle and species-energy theory, address the relationships between the rate of biological energy capture and species-level fitness and richness. The maximum power principle postulates that the fitness of self-organizing systems increases when they are designed to maximize power intake and subsequent energy transformation (Lotka, 1922; Odum and

Pinkerton, 1955). Organisms growing as members of communities have been observed to have higher power, that is, rates of energy acquisition, compared with members grown alone (DeLong, 2008). In relation, the species-energy theory proposes a positive correlation between biological energy capture and a system's species richness (May, 1975; Wright, 1983; Hurlbert and Stegen, 2014). This collective theoretical framework suggests that, within photoautotrophically driven ecosystems, the rates of gross oxygenic photosynthesis and net primary productivity should drive a positive relationship with species diversity.

Although the relationship between community productivity and species diversity has been frequently investigated, a unifying consensus on the shape of the relationship is lacking (Rajaniemi, 2003; Bienhold *et al.*, 2012). Similar ecosystems show different productivity–diversity relationships depending on the spatial scale of observation (Chase and Leibold, 2002; Grace *et al.*, 2016). Spatial gradients of productivity are inherent to photoautotrophically driven ecosystems in which light is attenuated at a characteristic distance related to the physical structure of the ecosystem. Benthic microbial mats and biofilms are of

Correspondence: HC Bernstein or JJ Moran, Chemical and Biological Signature Science, Pacific Northwest National Laboratory, PO Box 999, MS-IN: P7-50, Richland, WA 99352, USA. E-mail: Hans.Bernstein@pnnl.gov or James.Moran@pnnl.gov  
Received 28 April 2016; revised 26 July 2016; accepted 5 August 2016; published online 1 November 2016

particular interest in this respect, as tight physical associations between cells and extracellular polymeric substances strongly attenuate light over short distances. These compact microbial ecosystems exhibit stratified biological organization created and controlled by steep photo- and geochemical gradients on sub-millimeter spatial scales (Jørgensen *et al.*, 1979; Ley *et al.*, 2006; Jensen *et al.*, 2011).

In this study, we evaluated the spatial relationships between productivity and diversity in a photosynthetic microbial mat. The goal was to determine how vertical gradients in community composition and associated micro-environmental conditions translate to productivity. The experimental microcosm was derived from a benthic microbial mat native to epsomitic Hot Lake; located in Washington State, USA (Anderson, 1958; Lindemann *et al.*, 2013; Zachara *et al.*, 2016). Productivity was assessed by two spatially resolved, complementary metrics: the gross rate of oxygenic photosynthesis and %C replacement of biomass over time. The measured gross rate of oxygenic photosynthesis was used as an upper bound of photosynthetic energy acquisition. We evaluated the net rate of primary productivity at similar spatial scales using laser ablation isotope ratio mass spectrometry that enabled quantification of accumulation of  $^{13}\text{C}$ , derived from labeled  $\text{HCO}_3^-$ , into microbial biomass (Moran *et al.*, 2014). Both photosynthesis and net primary productivity were powered by absorption of light energy, which was inherently constrained to the photic zone, and regions of highest productivity exhibited relatively low-species richness but high evenness. Hence, this system exhibited negative-productivity richness and energy-richness relationships.

## Materials and methods

### *Cultures and media*

Microbial mats were sampled from the previously described Hot Lake field site (Lindemann *et al.*, 2013). Whole-mat samples and underlying sediment were transferred under dark, cool (4–10 °C) conditions. Each microcosm was maintained under 12:12 h light:dark cycles, illuminated at 150  $\mu\text{mol photons m}^{-2} \text{ sec}^{-1}$  (see spectrum Supplementary Figure S6) and fully submerged in a modified BG-11 media containing (mM): 120  $\text{Na}_2\text{SO}_4$ , 30 KCl, 0.187  $\text{NH}_4\text{Cl}$ , 600  $\text{MgSO}_4 \cdot 7\text{H}_2\text{O}$ , 0.0057  $\text{K}_2\text{HPO}_4$ , 0.245  $\text{CaCl}_2 \cdot 2\text{H}_2\text{O}$ , 0.0028 disodium EDTA and supplemented to 1  $\text{mM l}^{-1}$  with the following trace mineral solution (mM): 46.25  $\text{H}_3\text{BO}_3$ , 0.009  $\text{MnCl}_2 \cdot 4\text{H}_2\text{O}$ , 0.772  $\text{ZnSO}_4 \cdot 7\text{H}_2\text{O}$ , 1.61  $\text{Na}_2\text{MoO}_4 \cdot 2\text{H}_2\text{O}$ , 0.316  $\text{CuSO}_4 \cdot 5\text{H}_2\text{O}$ , 0.00017  $\text{Co}(\text{NO}_3)_2 \cdot 6\text{H}_2\text{O}$ .

### *Microcosm incubation*

A custom flow cell was constructed (BioSurface Technologies, Bozeman, MT, USA) for continuous

renewal of fresh media and mitigation of batch effects. Incubations were performed in experimental duplicate each containing four flow cells operated in parallel. Every measurement presented in this study was performed in a minimum of three biological replicates. The flow cell module consisted of a black aluminum housing containing four  $14.9 \times 3.8 \times 3.3$  cm chambers covered by gasket lids exposing a  $2.5 \times 9$  cm area (centered borosilicate glass window) that directed incident irradiance to the mat surface. Media was delivered at very low, laminar flows ( $1.7 \text{ ml min}^{-1}$  per chamber) to minimize shear. The overlaying liquid depth was controlled (1 cm) and mat samples were incubated on a 2 mm bed of sterile (autoclaved), native sediment. Sterile media entered a pre-mixing continuous stirred tank reactor upstream of the flow cell that was used to control temperature (22 °C), pH 7.5 and gas composition of the media during the incubation phase. Media delivery to the system was performed by two distinct protocols. First, during an acclimation phase (14 days of flow) the continuous stirred tank reactor was sparged at  $1 \text{ l min}^{-1}$  air enriched with 1%  $\text{CO}_2$ . The second, experimental phase, was performed over the last 24 h diel cycle to measure net primary productivity;  $^{13}\text{C}$  labeled  $\text{HCO}_3^-$  was introduced by replacing the continuous stirred tank reactor input for a carboy containing pH-adjusted (7.5) sterile media with 20 mM  $\text{NaHCO}_3$  at a 4:1 ratio of natural isotope abundance and  $^{13}\text{C}$ -labeled substrate. The labeled media was primed into the flow cell at high flow rates ( $\sim 170 \text{ ml min}^{-1}$ ) to mitigate dilution effects upon introduction. The  $^{13}\text{C}$ -labeled media was introduced at the beginning of a 12 h dark cycle to enable labeled  $\text{HCO}_3^-$  permeation through the mat in the absence of photosynthetic activity corresponding to negligible carbon fixation.

### *Micro-profiling*

Depth profiles of  $\delta^{13}\text{C}$  (‰) were sampled and measured in triplicate from cross sections of mat excised over the incubation time course. As previously described, lyophilized cross sections of these samples were analyzed using laser ablation sampling (Cetac LSX-500 laser ablation system, Omaha, NE, USA) coupled to isotope ratio mass spectrometry (Thermo Delta V plus isotope ratio mass spectrometer, Waltham, MA, USA) at sub-millimeter resolution (50–300  $\mu\text{m}$ ); the most common step size was 250  $\mu\text{m}$  (Moran *et al.*, 2011, 2014). Porosity profiles were measured in excised mat using nuclear magnetic resonance imaging (Renslow *et al.*, 2013). Briefly,  $^1\text{H}$  nuclear magnetic resonance was performed using a Bruker Avance III spectrometer (Bruker Biospin, Billerica, MA, USA) at 500 MHz, with imaging gradients (Bruker Micro2.5). Samples were positioned on agar in 15 mm nuclear magnetic resonance tubes, and degassed under dark conditions to remove bubbles prior to interrogation. ParaVision v5.1 was used to run chemical shift

selective imaging (mic chess) (Ha *et al.*, 2015; Lone *et al.*, 2015a) and 2D diffusion-mapping experiments (DtiStandard) (Lone *et al.*, 2015b), both with a resolution of  $78 \times 156 \mu\text{m}$ . Scalar irradiance (photosynthetically active radiation) profiles were measured in quadruplicate with isotropic photosynthetically active radiation microsenors with spherical  $70 \mu\text{m}$  diameter tips (Zensor, Åls-gårde, DK) fiber optically connected to a spectrophotometer (USB2000+-ES, Ocean Optics, Dunedin, FL, USA) and inter-calibrated against a radiometer (LI-250A and LI-COR Quantum sensor, LI-COR Biosciences, Lincoln, NE, USA) (Lassen *et al.*, 1992).  $\text{O}_2$  and gross photosynthesis rate profiles were measured in triplicate by previously described steady-state and light-dark shift methods (Glud *et al.*, 1992; Kühl *et al.*, 1996; Bernstein *et al.*, 2014). Briefly, Clark-type oxygen microsenors with  $25 \mu\text{m}$  tip diameter,  $<5\%$  stirring sensitivity and  $90\%$  response in  $<0.5 \text{ s}$  (OX-25 fast, Unisense A/S, Aarhus, Denmark) were used. Data acquisition and sensor positioning were facilitated by a multimeter and a manual micromanipulator fixed to a motorized stage connected with a PC laptop running software packages SensorTrace Suite and OceanView (Unisense A/S and Ocean Optics, respectively). The surface of the mat, relative depth = 0, was determined by activity. Only the mat was profiled via the methods described above and sediment was washed from the mat and discarded for each destructive sampling procedure.

#### Amplicon sequencing

The mat samples were excised from the flow cell at the conclusion of the 24 h label  $\text{HCO}_3^-$  incubation. The depth-wise cryosectioning, DNA extraction and DNA sequencing methods were performed as previously described (Lindemann *et al.*, 2013). Briefly, triplicate mat samples were embedded in sucrose, flash-frozen and cryosectioned into  $0.5 \text{ mm}$  vertical subsamples used for triplicate for genomic DNA extractions. Sequencing was done on an Illumina MiSeq (San Diego, CA, USA) instrument at the Joint Genome Institute, Walnut Creek, CA. Three separate 16S rRNA amplification reactions were performed for each extraction using the V4 forward primer (515F) and V4 reverse primer (806R) with 0–3 random bases and the Illumina sequencing primer binding site (Caporaso *et al.*, 2010). MiSeq data are available as study 10481 on Qiita (<https://qiita.ucsd.edu/study/description/10481>).

#### Amplicon analysis

Illumina reads were processed with QIIME 1.9.1 and VSEARCH 1.9.10, an open-source implementation of USEARCH (Caporaso *et al.*, 2010; Edgar, 2010; Rognes *et al.*, 2016). Overlapping reads were paired, trimmed to the V4 region, filtered to a maximum expected error rate of  $0.5 \text{ bp}$  per read and labeled.

Reads were pooled, de-replicated and chimera-checked with UCHIME *de novo* (Edgar *et al.*, 2011). After discarding chimeras and singletons, reads were clustered into OTUs at  $97\%$  similarity and an OTU table was constructed by mapping all labeled reads to these clusters. Taxonomy was assigned to each OTU centroid using the May 2013 version of the Greengenes database and a last common ancestor approach as implemented in QIIME 1.9.1 (McDonald *et al.*, 2012). Centroids were then aligned to Greengenes and a phylogenetic tree was constructed using FastTree (Price *et al.*, 2010). The relative abundances of taxa were compared and sorted as shown in Supplementary Data sets 1 and 2.

#### Phylogenetic diversity analysis

Downstream analysis was completed in R, using the phyloseq and vegan packages (Oksanen *et al.*, 2007; McMurdie and Holmes, 2013). Samples were rarified to an even depth after discarding samples with  $<22 \text{ K}$  reads. The rarified abundance counts were used for all measurements of alpha diversity (richness and evenness) and beta diversity, whereas the relative abundances of un-rarified samples were used for abundance-depth profiles (Figure 1a and Supplementary Figure S4). Weighted UniFrac distances were used to characterize beta diversity via canonical analysis of principle components (Anderson and Willis, 2003), whereas counts of unique OTUs and Simpson's E (evenness) were used to characterize alpha diversity (Hamady *et al.*, 2010). Methods to recreate this analysis are available in a GitHub repository (<https://github.com/pnnl/bernstein-2016-productivity-and-diversity>).

## Results

#### Depth profiles of taxa and environmental properties

Taxonomic abundance profiles showed a gradient in community composition over depth at sub-mm resolution (Figure 1a). Collectively, the mat harbored very-high bacterial diversity, with representatives of 51 phyla, dominated by members of *Cyanobacteria* and *Proteobacteria*. The three most abundant taxa, averaged over all positions and grouped at the order level, belonged to *Pseudanabaenales* (31.6%), *Rhodospirillales* (15.8%) and *Rhodobacterales* (9.8%). Taxonomic abundance profiles correlated with several measured profiles representing environmental properties or microbial productivity. Nine of the ten most abundant taxa, grouped at the class level, showed a positive correlation with depth and increased in abundance toward the bottom of the system (Supplementary Figure S1). The exception was observed for a cyanobacterium of class *Oscillatoriothycideae* that showed the inverse trend.

Steep gradients of dissolved  $\text{O}_2$  were measured and ranged from  $1540 \mu\text{M}$  within the top  $2 \text{ mm}$  to values near air saturation ( $255 \mu\text{M}$ ) at the base of



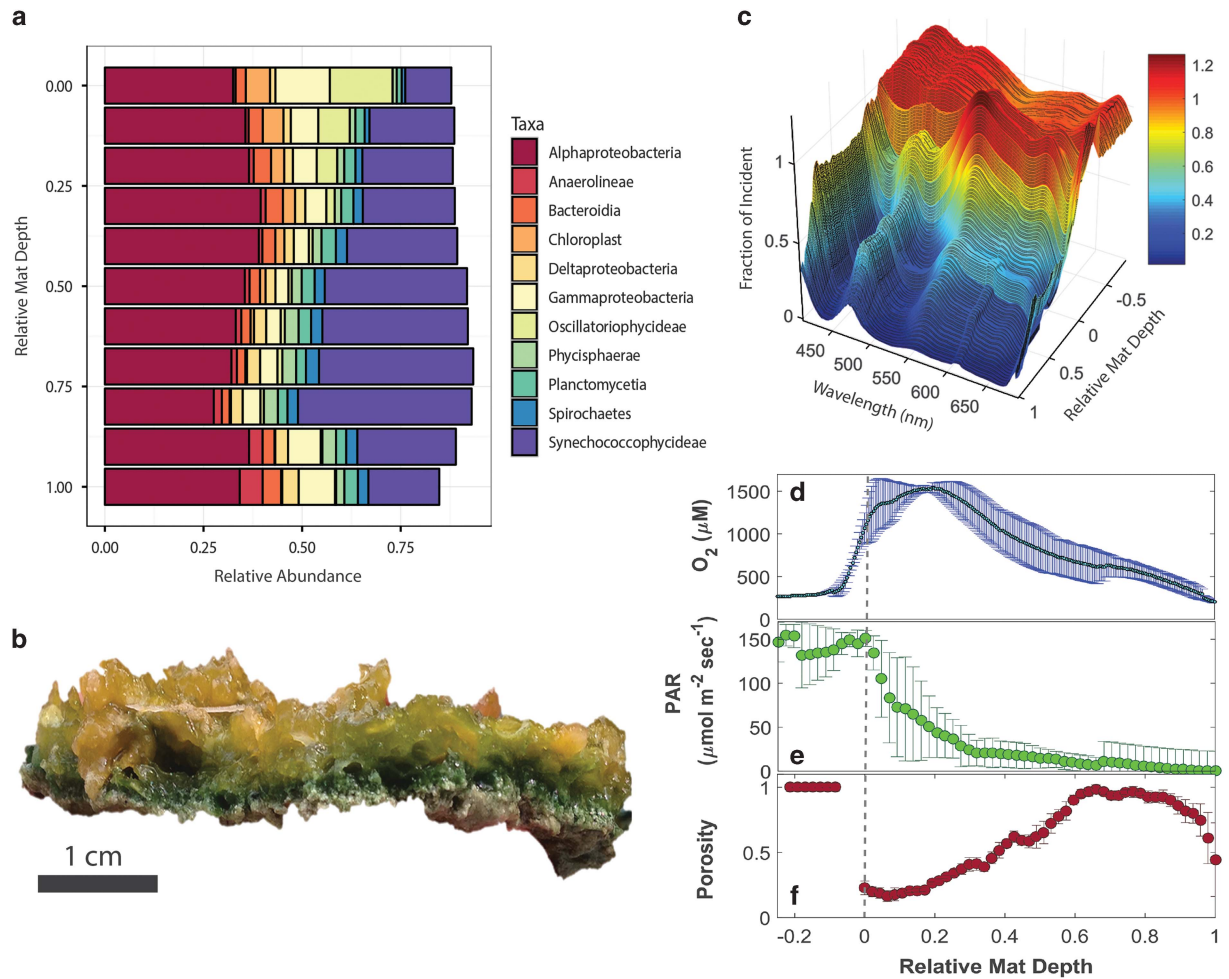


**Figure 1** The community and its environment. (a) Depth profile for the relative abundance of common taxa represented at the class level. (b) An excised microcosm of the benthic microbial ecosystem investigated. (c) Depth profile for spectral irradiance. (d) The dissolved O<sub>2</sub> profile. (e) The scalar irradiance (PAR) profile. (f) The porosity profile. Error bars represent  $\pm 1$  s.d. from  $\geq$  triplicate profile measurements. All depth profiles are reported as relative mat depth, which represents each position normalized by the total mat depth ( $1.05 \pm 0.4$  cm). PAR, photosynthetically active radiation.

the mat (Figure 1d). Depth profiles of spectral and scalar irradiance also varied over depth with wavelengths corresponding to chlorophyll *a* absorption preferentially attenuated (Figure 1c). Scalar incident irradiance of photosynthetically active radiation ( $150 \mu\text{mol photons m}^{-2} \text{sec}^{-1}$ ) was attenuated to  $\leq 10 \mu\text{mol photons m}^{-2} \text{sec}^{-1}$  at a depth of 2.6 mm and fully attenuated at 4.4 mm (0.41 relative depth) (Figure 1e). The physical structure of this system also exhibited microscale heterogeneity. This was determined by measuring the porosity of the mat, at  $\mu\text{m}$ -scale resolution, which increased with depth indicating that the surface was associated with less pore space, hence more resistant to mass transfer and light transmittance as compared with the bottom lamina (Figure 1f).

#### Depth-resolved community productivity

We quantified net primary productivity and gross oxygenic photosynthesis at sub-mm scales to

determine local community-level rates of carbon and energy acquisition. Net primary productivity was measured by spatiotemporally tracking the accumulation of <sup>13</sup>C, derived from a labeled HCO<sub>3</sub><sup>-</sup>, into biomass. The %C replacement through the mat depth profile over 24 h incubation was calculated from direct measurements of  $\delta^{13}\text{C}$  (‰) performed by laser ablation isotope ratio mass spectrometry (Supplementary Figure S2). Changes of biomass  $\delta^{13}\text{C}$  over the initial 12 h dark period were negligible (Supplementary Figure S3); indicating that photoautotrophy was the only measurable means for the community to acquire new carbon over the course of these incubations. Time course sampling over the following 12 h light period showed the greatest %C replacement near the surface of the mat (Figure 2a) and that net primary productivity was essentially limited to the photic zone ( $< 2.6$  mm depth).

The only exogenous energy input to the community was from light. Hence, the gross rate of oxygenic

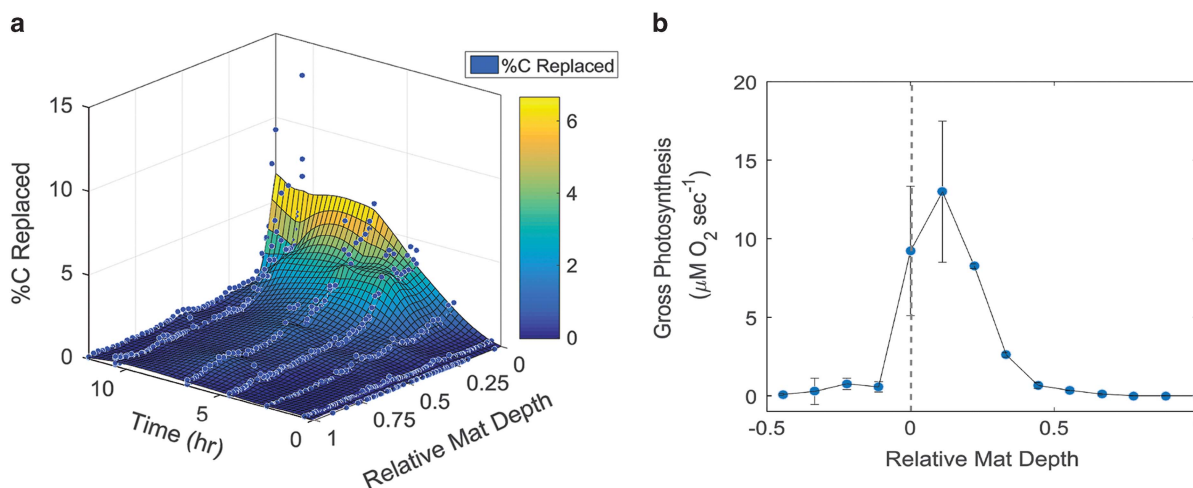


**Figure 2** Heterogeneous depth profiles of productivity. (a) Net primary productivity as determined by  $^{13}\text{C}$  accumulation, denoted as %C replaced in the biomass pool over a 24 h incubation with labeled  $\text{HCO}_3^-$  (12:12 h, light: dark cycle); all data are plotted from three replicate profile measurements. (b) The gross rate of oxygenic photosynthesis; error bars represent  $\pm 1$  s.d. from triplicate profile measurements. All depth profiles are reported as relative mat depth, which represents each position normalized by the total mat depth ( $1.05 \pm 0.4$  cm).

photosynthesis serves as a measure of biological energy acquisition. The profile of oxygenic photosynthesis showed a characteristic maximum just below the surface and decreased to negligible rates ( $< 0.1 \mu\text{M O}_2 \text{ h}^{-1}$ ) between 2 and 3 mm ( $\sim 0.26$  relative depth) (Figure 2b). Micro-profiles of each measure for productivity were fully coupled and correlated with scalar irradiance profiles of Supplementary Figure S1. By comparing the irradiance profile against gross photosynthesis, it was concluded that oxygenic photosynthesis ceased between scalar irradiances 40 and  $10 \mu\text{mol photons m}^{-2} \text{ sec}^{-1}$ .

Resource transfer from the photic zone to the deeper sections of the mat is an important process to consider for the ecology of the full mat system. When the net primary productivity and  $^{13}\text{C}$  enrichment profiles (Figure 2a, Supplementary Figures S2 and S3) are compared with the steady-state scalar irradiance profile (Figure 1e), it is clear that no significant amount of autotrophically derived carbon was transferred below the photic zone over the 24 h incubation. This result indicates that the time scale for exogenous carbon to be fixed and transferred into deeper sections of the mat (below relative depth of 0.41 or  $\sim 4.4$  mm) is much slower than the rate of net primary productivity.

#### Depth-resolved microbial diversity

Within the photic zone, where primary productivity occurs, the microbial mat exhibited a negative correlation between species richness and productivity (Figure 3 and Supplementary Table S1). Positions corresponding to the highest irradiance and greatest productivities showed relatively low-species richness. Interestingly, we observed an inverse relationship between community evenness and productivity. The rarefied subsamples exhibited a non-linear

gradient for the number of OTUs observed at each depth position (Figure 3a). The highest-species richness was observed at the bottom of the mat and the lowest values were measured in the upper photic zone and the upper dark zone (as defined by photosynthetically active radiation). Species richness showed linear increases with decreasing productivity (both gross photosynthesis and net primary productivity) inside the photic zone (Figures 3b and c). Similarly, richness increased with decreasing irradiance; thereby exhibiting a negative richness energy profile (Figure 3e). Below the photic zone correlations between richness and productivity were absent or negligible (coefficient of determination  $< 0.02$ ; Supplementary Table S1). Taken together, the environment-richness profiles, inclusive of porosity and dissolved  $\text{O}_2$ , were bimodal with both positive and negative correlations inflecting at the base of the photic zone (Figures 3d and f). Dissolved  $\text{O}_2$  gradients did not share the same observable negative relationship with species richness as did oxygenic photosynthesis and irradiance; indicating that dissolved  $\text{O}_2$  is inherently a complex measure that includes transport as well as *in situ* production and consumption.

The biological and environmental properties associated with beta diversity were assessed by a canonical analysis of principal coordinates that considered weighted UniFrac distances (Lozupone and Knight, 2005) between rarefied samples (Figure 4). Dissimilarity between intra-mat samples became more pronounced as the spatial distance between them increased. However, the relative distance between samples was not the only driver of beta diversity. Each measure of productivity showed near identical contributions to the observed variance in community structure. These were also co-aligned with the vectors representing the

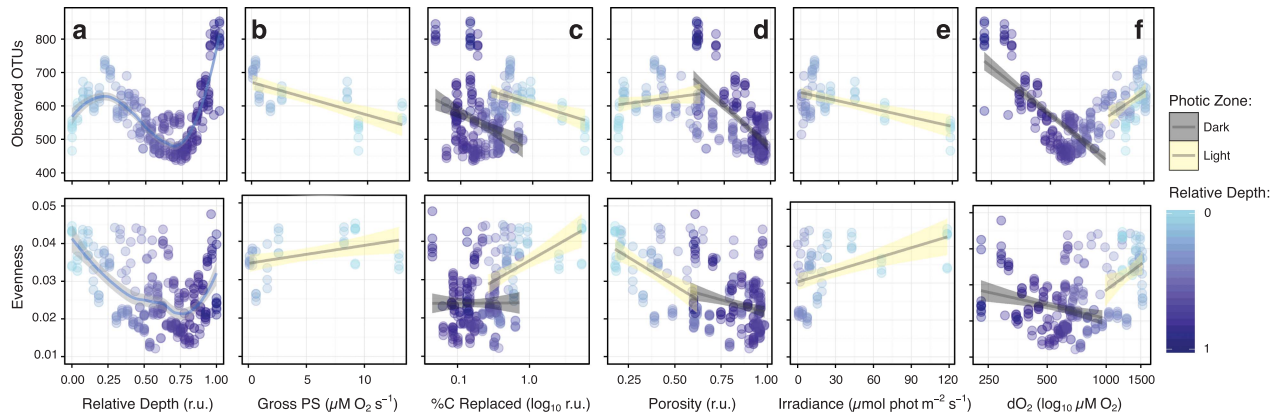


**Figure 3** Spatially resolved alpha diversity profiles. Species richness and evenness vary with: (a) relative mat depth; (b) the gross rate of oxygenic photosynthesis; (c) primary productivity; (d) porosity; (e) scalar irradiance (PAR); and (f) dissolved O<sub>2</sub>. Linear regression was performed on rarefied samples corresponding to positions within the photic zone (yellow lines) and in the ‘dark’ zone (gray lines). The shaded regions, around each line, represent  $\pm 1$  s.e. PAR, photosynthetically active radiation.

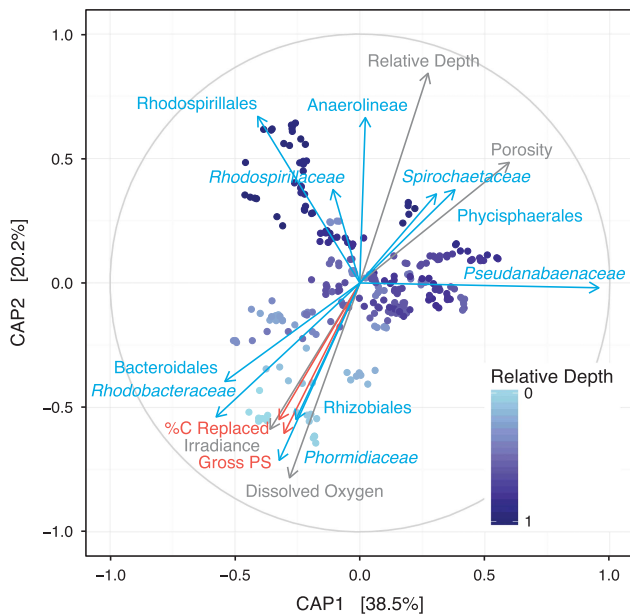


**Figure 4** Beta diversity. Canonical analysis of principal coordinates (CAP) of weighted UniFrac distances between rarefied samples. These two principle components capture more than 55% of the variance observed. Each vector has a magnitude (length) sign (direction) of a variable’s contributions to the principle components. Vectors represent: profiles for each measure of productivity (red), profiles of environmental properties (gray) and the most common taxa (blue). After merging OTUs at the family level, the ten most abundant families are shown here labeled at the family level (italics) or at a higher taxonomic level.

contributions of scalar irradiance and dissolved O<sub>2</sub> to beta diversity. These properties are maximal at the mat’s upper surface, a region that exhibits relatively high productivity, low-species richness and high community evenness. Members of *Phormidiaceae* and of an unidentified family of the order *Rhizobiales* varied in the same direction as productivity. Reads from family *Phormidiaceae* were dominated by an OTU that exhibited 100% identity to

previously identified filamentous cyanobacterium *Phormidium* sp. OSCR, cultivated within a consortium from the Hot Lake mat (Cole *et al.*, 2014). *Rhodobacteraceae* and the *ML635J-40* family of the order *Bacteroidales* also varied in the same direction as productivity. An abundant member in family *Rhodobacteraceae* was an identical match to a previously described *Roseibacterium* sp. HL7711\_P4H5, also a member of the Hot Lake uncyanobacterial consortia (Cole *et al.*, 2014).

## Discussion

The aim of this study was to use a controlled incubation of a naturally derived, photoautotrophically driven microbial community to interrogate the spatially resolved relation between microbiome diversity and productivity. We combined sub-millimeter depth profiles of net primary productivity and gross oxygenic photosynthesis with amplified 16S rRNA sequences to demonstrate a link between relatively high diversity in regions of the photic zone corresponding to low overall productivity. The Hot Lake microbial mat was ideal for studying relationships between productivity and diversity because of its high bacterial diversity and pronounced gradients of chemical and physical properties that differentiate niche spaces.

The controlled microcosm experiment allowed us to examine the spatially resolved relation between microbial diversity with community energy and carbon acquisition via methods, such as stable isotope probing, that are much more difficult *in situ*. Because the mat community was maintained under laboratory conditions, we qualify the inferences made here on two assumptions. The first is that sufficient time had passed for the community to acclimate to its controlled environment such that equilibrium, with respect to community structure, was obtained. The inferred relationships between



diversity and productivity are limited to the effect that species richness, evenness and position-specific community structures have on productivity but not the reverse. It is important to note that the relationships observed here do not explicitly inform the directionality or causation. The second assumption is that as this community is driven by photoautotrophic productivity and it is light energy controlled. This assumption is partially supported by the experimental design; acclimation of the system to inorganic medium with light as the sole energy source. This was further supported by the observation that a measurable enrichment of  $^{13}\text{C}$  in microbial biomass was not detected in the deeper, dark sections of the mat or by the end of the 12 h dark incubation. Ultimately the rates of photosynthetic electron acquisition and net primary productivity will set the upper limit for community productivity through the entire mat system. All depth positions in the mat clearly include diverse taxa representing chemo- and photoheterotrophic lifestyles. The relationships between diversity and heterotrophic productivity, driven by exchanges of energy and carbon between the photic zone and deeper dark sections of the mat, were not quantified here and may have spatial patterns distinct from those measured in the photic zone.

#### *Diversity–productivity relationships*

Although the diversity of microbial mat ecosystems has been an intense area of investigation, this current study uniquely focuses on spatial trade-offs between diversity and productivity. This study revealed localized negative-productivity richness and negative-energy richness relationships, each observed through sub-millimeter depth profiles. Although explicit investigations of microbial diversity–productivity relationships are rarely reported, spatially resolved profiles of diversity have been characterized in other hypersaline microbial mat systems. Of these include the comparable microbial mats of Guerrero Negro (Baja California Sur, Mexico), which have historically been of keen interest as spatially stratified, highly diverse model microbial ecosystems (Canfield and Des Marais, 1993; Risatti *et al.*, 1994; Ley *et al.*, 2006). A previous study reported increasing OTU counts with depth over the first 3 mm of the Guerrero Negro mat (Harris *et al.*, 2013). Although depth profiles of productivity were not explicitly measured, higher-species richness presumably corresponded with lower rates of photosynthesis than would be observed at the mat's surface. In contrast, another comparable ecosystem from Shark Bay (Australia) reported a decreasing species richness down from the surface of the mat into the first 4 mm (Wong *et al.*, 2015). Observations of gross oxygenic photosynthesis from Wong *et al.* (2015) Shark Bay study were collected by the same light–dark shift method as reported in the current study; hence, by our same metric, the system

exhibited a positive-productivity richness relationship. The Guerrero Negro and Shark Bay mats are comparable to current Hot Lake system in that they are highly diverse, stratified, hypersaline microbial ecosystems abundant in cyanobacteria. However, the current Hot Lake system distinctly represents an epsomitic hypersaline habitat (that is, 400 mM  $\text{MgSO}_4$ ) dominated by divalent ions as compared with the marine, NaCl-based hypersaline systems. If it is assumed that the depth profiles of gross oxygenic photosynthesis and net primary productivity are similar across stratified cyanobacterial mat ecosystems, then a comparative survey of results reported allows a conclusion to be drawn that similar microbial ecosystems show different productivity–diversity curves; a supposition that has long been established in macro-ecology.

Energetic constraints underpin the productivities of all ecosystems. Empirical observations have supported the concept that biologically available energy, which is typically inclusive of resource availability and productivity, may also limit species richness (Hurlbert and Stegen, 2014). Positive species–energy relationships have been investigated at the field and lab scales (Srivastava and Lawton, 1998; Hurlbert, 2006). However, the species–energy theory has largely been examined from an macro-ecological framework and remains nascent within microbial ecology as a discipline; but see discussions by Prosser *et al.*, 2007. An exception to this has been presented in a study focused on the energy–diversity relationships in arctic seafloor microbial ecosystems (Bienhold *et al.*, 2012). This study reported overall positive relationships between species richness and energy availability provided in the form of photosynthetically derived detritus. This microbe-specific positive species–energy relationship was established by considering chemotrophic community diversity (deep sea sediment) in the context of trophic energy exchanges from photosynthetic primary producers. This is also common for macro-ecological studies that have reported positive species–energy relationships that consider inputs from light energy, as demonstrated by studies focused on species richness of birds and mammals (Turner *et al.*, 1988; Wylie and Currie, 1993). Our current study differs in that a negative species–energy relationship was observed by including the contributions to species richness made by the cosmopolitan, photoautotrophic primary producers.

Biologically available energy, exogenous to the current system, was solely delivered by actinic light. Hence, the negative species–energy relationship, observed in the photic zone of this system, was indeed rare and in disagreement with the species–energy theory. This also holds true when biologically available ‘energy’ is considered by a broader definition that includes productivity. Other spatially stratified light-driven microbial ecosystems, beyond mats, may also exhibit negative diversity–energy relationships. For example, a well-studied

meromictic Lake in Antarctica (Ace Lake) reported an increasing microbial diversity depth profile over 23 m (Lauro *et al.*, 2011). The Ace lake system is highly abundant in green sulfur bacteria and their role as primary producers in the system is apparent; however, the spatial locations corresponding to the highest diversity of the system are in the deeper strata that would presumably have low net primary productivity. Negative species–energy relationships may be indicative of stratified light-driven ecosystems that are able to be the most productive with a relatively smaller, even distribution of species that specialize within the photic zone.

#### *Specific taxa and biological niches*

Depth profiles of environmental properties, that is, dissolved O<sub>2</sub>, irradiance and porosity, uncovered a continuum of regions corresponding to specific biological niches. These niche spaces mapped to common taxa that were associated with measured variance in community structure (beta diversity shown in Figure 4). Some OTUs, belonging to the most abundant families (Supplementary Figure S5), matched species that have been previously described and sequenced (Cole *et al.*, 2014; Nelson *et al.*, 2016) allowing function, relating to microbial lifestyle and niche space, to be inferred. The *Phormidium* sp. OSCR-like OTU was inferred to be a major primary producer based on close alignment of *Phormidiaceae* depth profiles with each measure of productivity. Interestingly, this cyanobacterium is known to be motile and metabolically coupled to heterotrophic bacteria that match or are very similar to the OTUs abundant near the surface of the mat, for example, *Roseibacterium* sp. HL7711\_P4H5 (Cole *et al.*, 2014; Nelson *et al.*, 2016). The most abundant OTU identified in this system belonged to a cyanobacterium of the family *Pseudanabaenaceae*. The abundance of this cyanobacterium was maximal in the dark zone, corresponding to low-species richness and low evenness. Hence, we infer that *Pseudanabaenaceae* may be light sensitive and/or capable of operating as an aerobic heterotroph just below the photic zone. Another possibility is that it and other taxa are non-motile and thereby trapped within the microcosm that that does not experience the high irradiances possible from solar noon (~2000  $\mu\text{mol photons m}^{-2} \text{ sec}^{-1}$ ) in the natural habitat (Lindemann *et al.*, 2013).

*Roseibacterium* sp. HL7711\_P4H5 (family *Rhodobacteraceae* matching to OTU-21) has been characterized as a heterotroph on medium containing *N*-acetylglucosamine as the sole carbon source and can grow on photosynthate derived from *Phormidium* sp. OSCR (Cole *et al.*, 2014). A *Rhizobiales* sp. ACL\_P1B5-like OTU (OTU-22) is predicted to be an aerobic photoheterotroph capable of catabolizing organic acids and carbohydrates. Members of a related, but unidentified, family of order *Rhizobiales* corresponded closely with

increasing productivity measures, dissolved O<sub>2</sub>, irradiance and the cyanobacterial family *Phormidiaceae*. Taxa that showed increasing relative abundance profiles with mat depth did not match with Hot Lake-derived strains previously characterized in the culture. Interestingly, OTUs belonging to the class *Anaerolineae* have largely been described as obligate anaerobes (Yamada *et al.*, 2006; Narihiro and Kamagata, 2013) and were among the most abundant families in the bottom sections of the mat. Anaerobic metabolism of associated taxa may have been maintained by the 12 h diel cycle imposed on the experiment.

## Conclusions

Of the most fundamental ecological attributes of any system include the biotic rates of carbon and energy acquisition and the resulting number of species this can support. Here we presented a study designed to capture the heterogeneous spatial relationships between microbiome diversity and productivity. The primary result was that this system exhibited a negative species productivity and energy relationships. It should be noted that the inferences garnered here are limited based on empirical relationships derived from multivariate data. Foremost among these limitations is that correlation does not imply causation. The current study does, however, report a unique microscale spatial investigation of microbial productivity as it relates to culture-independent molecular methods that characterize bacterial diversity. In part, this new level of spatial resolution for productivity is due to the novel application of laser ablation isotope ratio mass spectrometry technology that enabled sub-micron scale measurements of <sup>13</sup>C enrichment and net primary productivity. This study provides new context for an underrepresented area of microbial ecology by uncovering sub-millimeter scale spatial relationships between microbial diversity and productivity.

## Conflict of Interest

The authors declare no conflict of interest.

## Acknowledgements

This research was supported by the US Department of Energy Office of Biological and Environmental Research (BER) Genomic Science Program and is a contribution of the Fundamental Scientific Focus Area. The work conducted by the U.S. DOE Joint Genome Institute was supported by the Office of Science of the U.S. DOE under contract No. DE-AC0205CH11231 and Community Sequencing Project 701. HCB and RSR are grateful for support given by the Linus Pauling Distinguished Postdoctoral Fellowship, a Laboratory Directed Research program at PNNL. We wish to acknowledge William P. Inskeep, William C. Nelson, James C. Stegen and Jennifer M. Moberley for helpful discussions and critical review of



this study. PNNL is operated for the DOE by Battelle Memorial Institute under Contract DE-AC05-76RLO 1830.

## References

- Anderson G. (1958). Some limnological features of a shallow saline meromictic lake. *Limnol Oceanogra* **3**: 259–270.
- Anderson MJ, Willis TJ. (2003). Canonical analysis of principal coordinates: a useful method of constrained ordination for ecology. *Ecology* **84**: 511–525.
- Bernstein HC, Kesaano M, Moll K, Smith T, Gerlach R, Carlson RP *et al.* (2014). Direct measurement and characterization of active photosynthesis zones inside wastewater remediating and biofuel producing microalgal biofilms. *BioresTechnol* **156**: 206–215.
- Bienhold C, Boetius A, Ramette A. (2012). The energy–diversity relationship of complex bacterial communities in Arctic deep-sea sediments. *ISME J* **6**: 724–732.
- Canfield DE, Des Marais DJ. (1993). Biogeochemical cycles of carbon, sulfur, and free oxygen in a microbial mat. *Geochim Cosmochim Acta* **57**: 3971–3984.
- Caporaso JG, Kuczynski J, Stombaugh J, Bittinger K, Bushman FD, Costello EK *et al.* (2010). QIIME allows analysis of high-throughput community sequencing data. *Nat Methods* **7**: 335–336.
- Chase JM, Leibold MA. (2002). Spatial scale dictates the productivity–biodiversity relationship. *Nature* **416**: 427–430.
- Cole JK, Hutchison JR, Renslow RS, Kim Y-M, Chrisler WB, Engelmann HE *et al.* (2014). Phototrophic biofilm assembly in microbial-mat-derived unicyanobacterial consortia: model systems for the study of autotroph–heterotroph interactions. *Front Microbiol* **5**: 109.
- DeLong JP. (2008). The maximum power principle predicts the outcomes of two-species competition experiments. *Oikos* **117**: 1329–1336.
- Edgar RC. (2010). Search and clustering orders of magnitude faster than BLAST. *Bioinformatics* **26**: 2460–2461.
- Edgar RC, Haas BJ, Clemente JC, Quince C, Knight R. (2011). UCHIME improves sensitivity and speed of chimera detection. *Bioinformatics* **27**: 2194–2200.
- Field CB, Behrenfeld MJ, Randerson JT, Falkowski P. (1998). Primary production of the biosphere: integrating terrestrial and oceanic components. *Science* **281**: 237–240.
- Glud RN, Ramsing NB, Revsbech NP. (1992). Photosynthesis and photosynthesis-coupled respiration in natural biofilms quantified with oxygen microsensors. *J Phycol* **28**: 51–60.
- Grace JB, Anderson TM, Seabloom EW, Borer ET, Adler PB, Harpole WS *et al.* (2016). Integrative modelling reveals mechanisms linking productivity and plant species richness. *Nature* **529**: 390–393.
- Ha PT, Renslow RS, Atci E, Reardon PN, Lindemann SR, Fredrickson JK *et al.* (2015). Regulation of electron transfer processes affects phototrophic mat structure and activity. *Front Microbiol* **6**: 909.
- Hamady M, Lozupone C, Knight R. (2010). Fast UniFrac: facilitating high-throughput phylogenetic analyses of microbial communities including analysis of pyrosequencing and PhyloChip data. *ISME J* **4**: 17–27.
- Harris JK, Caporaso JG, Walker JJ, Spear JR, Gold NJ, Robertson CE *et al.* (2013). Phylogenetic stratigraphy in the Guerrero Negro hypersaline microbial mat. *ISME J* **7**: 50–60.
- Hurlbert AH. (2006). Linking species–area and species–energy relationships in *Drosophila* microcosms. *Ecol Lett* **9**: 287–294.
- Hurlbert AH, Stegen JC. (2014). When should species richness be energy limited, and how would we know? *Ecol Lett* **17**: 401–413.
- Jensen SI, Steunou A-S, Bhaya D, Kühl M, Grossman AR. (2011). *In situ* dynamics of O<sub>2</sub>, pH and cyanobacterial transcripts associated with CCM, photosynthesis and detoxification of ROS. *ISME J* **5**: 317–328.
- Jørgensen BB, Revsbech NP, Blackburn TH, Cohen Y. (1979). Diurnal cycle of oxygen and sulfide microgradients and microbial photosynthesis in a cyanobacterial mat sediment. *Appl Environ Microb* **38**: 46–58.
- Kühl M, Glud RN, Ploug H, Ramsing NB. (1996). Micro-environmental control of photosynthesis and photosynthesis-coupled respiration in an epilithic cyanobacterial biofilm. *J Phycol* **32**: 799–812.
- Lassen C, Ploug H, Jørgensen BB. (1992). A fibre-optic scalar irradiance microsensor: application for spectral light measurements in sediments. *FEMS Microbiol Lett* **86**: 247–254.
- Lauro FM, DeMaere MZ, Yau S, Brown MV, Ng C, Wilkins D *et al.* (2011). An integrative study of a meromictic lake ecosystem in Antarctica. *ISME J* **5**: 879–895.
- Ley RE, Harris JK, Wilcox J, Spear JR, Miller SR, Bebout BM *et al.* (2006). Unexpected diversity and complexity of the Guerrero Negro hypersaline microbial mat. *Appl Environmental Microb* **72**: 3685–3695.
- Lindemann SR, Moran JJ, Stegen JC, Renslow RS, Hutchison JR, Cole JK *et al.* (2013). The epsomitic phototrophic microbial mat of Hot Lake, Washington: community structural responses to seasonal cycling. *Front Microbiol* **4**: 323.
- Lone AG, Atci E, Renslow R, Beyenal H, Noh S, Fransson B *et al.* (2015a). Colonization of epidermal tissue by *Staphylococcus aureus* produces localized hypoxia and stimulates secretion of antioxidant and caspase-14 proteins. *Infect Immun* **83**: 3026–3034.
- Lone AG, Atci E, Renslow R, Beyenal H, Noh S, Fransson B *et al.* (2015b). *Staphylococcus aureus* induces hypoxia and cellular damage in porcine dermal explants. *Infect Immun* **83**: 2531–2541.
- Lotka AJ. (1922). Contribution to the energetics of evolution. *Proc Natl Acad Sci USA* **8**: 147–151.
- Lozupone C, Knight R. (2005). UniFrac: a new phylogenetic method for comparing microbial communities. *Appl Environ Microb* **71**: 8228–8235.
- May RM. (1975). Patterns of species abundance and diversity. *Ecol Evol Commun*, Harvard University Press: Cambridge, MA, USA, pp 81–120.
- McDonald D, Price MN, Goodrich J, Nawrocki EP, DeSantis TZ, Probst A *et al.* (2012). An improved Greengenes taxonomy with explicit ranks for ecological and evolutionary analyses of bacteria and archaea. *ISME J* **6**: 610–618.
- McMurdie PJ, Holmes S. (2013). phyloseq: an R package for reproducible interactive analysis and graphics of microbiome census data. *PLoS One* **8**: e61217.
- Moran JJ, Newburn MK, Alexander ML, Sams RL, Kelly JF, Kreuzer HW. (2011). Laser ablation isotope ratio mass spectrometry for enhanced sensitivity and spatial

- resolution in stable isotope analysis. *Rapid Commun Mass Spectrom* **25**: 1282–1290.
- Moran JJ, Doll CG, Bernstein HC, Renslow RS, Cory AB, Hutchison JR et al. (2014). Spatially tracking <sup>13</sup>C-labelled substrate (bicarbonate) accumulation in microbial communities using laser ablation isotope ratio mass spectrometry. *Environ Microbiol Rep* **6**: 786–791.
- Narihiro T, Kamagata Y. (2013). Cultivating yet-to-be cultivated microbes: the challenge continues. *Microbes Environ* **28**: 163–165.
- Nelson WC, Maezato Y, Wu Y-W, Romine MF, Lindemann SR. (2016). Identification and resolution of microdiversity through metagenomic sequencing of parallel consortia. *Appl Environ Microb* **82**: 255–267.
- Odum HT, Pinkerton RC. (1955). Time's speed regulator: the optimum efficiency for maximum power output in physical and biological systems. *Am Sci* **43**: 331–343.
- Oksanen J, Kindt R, Legendre P, O'Hara B, Stevens MHH, Oksanen MJ et al. (2007). The vegan package. Community ecology package. 10. Available at: <https://cran.r-project.org/web/packages/vegan/>.
- Price MN, Dehal PS, Arkin AP. (2010). FastTree 2—approximately maximum-likelihood trees for large alignments. *PLoS One* **5**: e9490.
- Prosser JI, Bohannon BJ, Curtis TP, Ellis RJ, Firestone MK, Freckleton RP et al. (2007). The role of ecological theory in microbial ecology. *Nat Rev Microbiol* **5**: 384–392.
- Rajaniemi TK. (2003). Explaining productivity-diversity relationships in plants. *Oikos* **101**: 449–457.
- Renslow RS, Babauta JT, Dohnalkova A, Boyanov MI, Kemner KM, Majors PD et al. (2013). Metabolic spatial variability in electrode-respiring *Geobacter sulfurreducens* biofilms. *Energy Environ Sci* **6**: 1827–1836.
- Risatti J, Capman W, Stahl D. (1994). Community structure of a microbial mat: the phylogenetic dimension. *Proc Natl Acad Sci USA* **91**: 10173–10177.
- Rognes T, Mahé F, Flouri T, McDonald D, Schloss P, Woodcroft BJ. (2016). VSEARCH: a versatile open source tool for metagenomics. *PeerJ Preprints* **6**: e2409v1. Available at: <https://doi.org/10.7287/peerj.preprints.2409v1>.
- Srivastava DS, Lawton JH. (1998). Why more productive sites have more species: an experimental test of theory using tree-hole communities. *Am Nat* **152**: 510–529.
- Turner JR, Lennon JJ, Lawrenson JA. (1988). British bird species distributions and the energy theory. *Nature* **335**: 539–541.
- Wong HL, Smith D-L, Visscher PT, Burns BP. (2015). Niche differentiation of bacterial communities at a millimeter scale in Shark Bay microbial mats. *Sci Rep* **5**: 15607.
- Wright DH (1983). Species-energy theory: an extension of species-area theory. *Oikos* **41**: 496–506.
- Wylie JL, Currie DJ. (1993). Species-energy theory and patterns of species richness: I. Patterns of bird, angiosperm, and mammal species richness on islands. *Biol Conserv* **63**: 137–144.
- Yamada T, Sekiguchi Y, Hanada S, Imachi H, Ohashi A, Harada H et al. (2006). *Anaerolinea thermolimosa* sp. nov., *Levilinea saccharolytica* gen. nov., sp. nov. and *Leptolinea tardivitalis* gen. nov., sp. nov., novel filamentous anaerobes, and description of the new classes Anaerolineae classis nov. and Caldilineae classis nov. in the bacterial phylum Chloroflexi. *Int J Syst Evol Microbiol* **56**: 1331–1340.
- Zachara JM, Moran JJ, Resch CT, Lindemann SR, Felmy AR, Bowden ME et al. (2016). Geo-and biogeochemical processes in a heliothermal hypersaline lake. *Geochim Cosmochim Acta* **181**: 144–163.

Supplementary Information accompanies this paper on the ISME Journal website (<http://www.nature.com/ismej>)